




## Article

# Automated Analysis of Australian Tropical Cyclones with Regression, Clustering and Convolutional Neural Network

Fahim Sufi <sup>1,\*</sup> , Edris Alam <sup>2,3</sup>  and Musleh Alsulami <sup>4</sup> 

<sup>1</sup> Federal Government, Melbourne, VIC 3000, Australia

<sup>2</sup> Faculty of Resilience, Rabdan Academy, P.O. Box 114646, Abu Dhabi 22401, United Arab Emirates

<sup>3</sup> Department of Geography and Environmental Studies, University of Chittagong, Chittagong 4331, Bangladesh

<sup>4</sup> Information Systems Department, Umm Al-Qura University (UQU), Makkah 24382, Saudi Arabia

\* Correspondence: research@fahimsufi.com

**Abstract:** Tropical cyclones take precious lives, damage critical infrastructure, and cause economic losses worth billions of dollars in Australia. To reduce the detrimental effect of cyclones, a comprehensive understanding of cyclones using artificial intelligence (AI) is crucial. Although event records on Australian tropical cyclones have been documented over the last 4 decades, deep learning studies on these events have not been reported. This paper presents automated AI-based regression, anomaly detection, and clustering techniques on the largest available cyclone repository covering 28,713 records with almost 80 cyclone-related parameters from 17 January 1907 to 11 May 2022. Experimentation with both linear and logistic regression on this dataset resulted in 33 critical insights on factors influencing the central pressure of cyclones. Moreover, automated clustering determined four different clusters highlighting the conditions for low central pressure. Anomaly detection at 70% sensitivity identified 12 anomalies and explained the root causes of these anomalies. This study also projected parameterization and fine-tuning of AI-algorithms at different sensitivity levels. Most importantly, we mathematically evaluated robustness by supporting an enormous scenario space of  $4.737 \times 10^{8234}$ . A disaster strategist or researcher can use the deployed system in iOS, Android, or Windows platforms to make evidence-based policy decisions on Australian tropical cyclones.

**Keywords:** Australian tropical cyclones; linear regression; logistic regression; anomaly detection; clustering cyclones; AI based cyclone analysis



**Citation:** Sufi, F.; Alam, E.; Alsulami, M. Automated Analysis of Australian Tropical Cyclones with Regression, Clustering and Convolutional Neural Network. *Sustainability* **2022**, *14*, 9830. <https://doi.org/10.3390/su14169830>

Academic Editor: Wen Cheng Liu

Received: 15 June 2022

Accepted: 6 August 2022

Published: 9 August 2022

**Publisher's Note:** MDPI stays neutral with regard to jurisdictional claims in published maps and institutional affiliations.



**Copyright:** © 2022 by the authors. Licensee MDPI, Basel, Switzerland. This article is an open access article distributed under the terms and conditions of the Creative Commons Attribution (CC BY) license (<https://creativecommons.org/licenses/by/4.0/>).

## 1. Introduction

The absolute monetary value of catastrophic events in Australia from 2006 to 2016 were found to cost \$18.2 billion every year, equating to about 1.2% of Australia's gross domestic product (GDP) [1]. A significant portion of these catastrophic events were tropical cyclones. For example, 100% of the economic loss from catastrophic events within Northern Territory was attributed to cyclones. On the other hand, about 25% of the economic loss in Queensland could be attributed to cyclones and hail [1]. In year 2060, the projected economic loss within Australia due to catastrophic events is between \$73 billion to \$94 billion, with 31% contribution from tropical cyclones [2]. To mitigate the impact of catastrophic events, it is imperative to aggregate, curate, dissect, analyze, and understand datasets containing catastrophic events. As stated by the United Nations, the main element of an effective and efficient early warning framework is "Disaster risk knowledge based on the systematic collection of data and disaster risk assessments" [3]. The adverse effects of tropical cyclones and other catastrophic events could be mitigated with AI-driven early warning systems, as well as simulation and modelling of catastrophic events for improved disaster preparedness [4,5].

In our latest review, we utilized artificial intelligence (AI) to obtain hidden insights from NASA's worldwide landslide incident database [6,7]. Moreover, we recently used

AI-based regression analysis such as linear and logistic regressions to identify and explain factors responsible for tornado-related casualties in Bangladesh [8,9]. We have also utilized AI to critically analyze casualties of landslides in Chittagong Metropolitan Area, Bangladesh [10]. Lastly, we used AI-based services and algorithms to automatically process social media posts of catastrophic events and obtained AI-driven insights from them [11,12]. Deep learning algorithms such as the convolutional neural network (CNN) were used to obtain a deep situational understanding of disasters (e.g., cyclones) [11,12]. It should be mentioned that all our recent studies (i.e., [6–12]) resulted in practical solutions that assisted disaster planners, strategists, and policy makers to make evidence-based practical decisions using their own devices (e.g., iOS, Android, or Windows).

Following the recommendations and advice of the United Nations [3], World Bank [5], and other international and national agencies, Australia has been actively monitoring, collecting, and analyzing tropical cyclones under the guidance of the Australian Government's Bureau of Meteorology for the last 4 decades [13–16]. Even though applications of AI [17] and deep learning-based studies with the artificial neural network (ANN) [18], deep neural network (DNN) [19], and CNN [11,12] have demonstrated significant advancement in analyzing cyclones, none of these advanced techniques have been applied to the Australian Tropical Cyclone databases in [13,14]. In this study, we reported an innovative use of automated machine learning algorithms involving CNN, linear regression, logistic regression, and k-means clustering to obtain deep intelligence on Australian tropical cyclones. The core contributions of this study include:

- This is the first study to report deep learning techniques with CNN on the Australian cyclone database [13,14].
- This paper reports the most comprehensive study involving cyclone datasets from 17 January 1907 to 11 May 2022, including 1067 Australian cyclones and 28,713 records with almost 80 cyclone-related parameters. The proposed methodology provides AI-based insights on over  $4.737 \times 10^{8234}$  scenarios.
- Using automated AI-driven regression analysis, we discovered and explained 33 factors or dimensions that directly influence decreases in central pressure.
- With automated k-means clustering, this is first study that answered strategic questions such as, “When is the central pressure of cyclones more likely to be low?” by discovering four clusters and ranking them (i.e., with respect to average central pressure).
- CNN-based deep learning automatically led to the discovery of 12 anomalies on Australian cyclone events with abnormally high wind speeds, at 70% sensitivity of the anomaly detection algorithm. Moreover, we reported detailed experimentation results on varying sensitivities of anomaly detection algorithms, which has never been reported in previous studies [8,9,15–18].
- Unlike previous studies in [8,9,15–18], this study generated a dashboard that would allow decision-makers to make strategic evidence-based policy decisions on Australian tropical cyclones. This dashboard was deployed on multiple platforms such as iOS, Android, and Windows, so that it could be easily adopted by disaster strategists, planners, and researchers.

In summary, this study focused on understanding the complex relations among various parameters related to Australian tropical cyclones to answer the following research questions:

- What factors influence a cyclone's central pressure?
- How do these factors create a cyclone with lower central pressure?
- How can we identify the characteristics of cyclone events with the lowest central pressure?
- When did we witness the strongest cyclones with the highest damage potential?
- What characteristics generate strong cyclones with higher wind speeds?

## 2. Materials and Methods

The cyclone events analyzed in this study were gathered and aggregated from [13,14]. The aggregated cyclone records were cleaned and transformed before being analyzed and

displayed. Furthermore, the data was modelled using best practices shown in [20]. Finally, our data was analyzed using AI algorithms on the Microsoft Power Platform [21]. Within this section, further details on data sourcing, study area, and AI algorithms are described. As seen in Figure 1, we first connected to the Australian cyclone dataset [13] using Microsoft Power Query. Then the data was modelled and visualized in Microsoft Power BI. Finally, we applied AI-based algorithms such as regression (both linear and logistic regression), clustering (k-means clustering), and anomaly detection (CNN-based deep learning) to obtain AI-driven insights from the Australian tropical cyclone dataset.

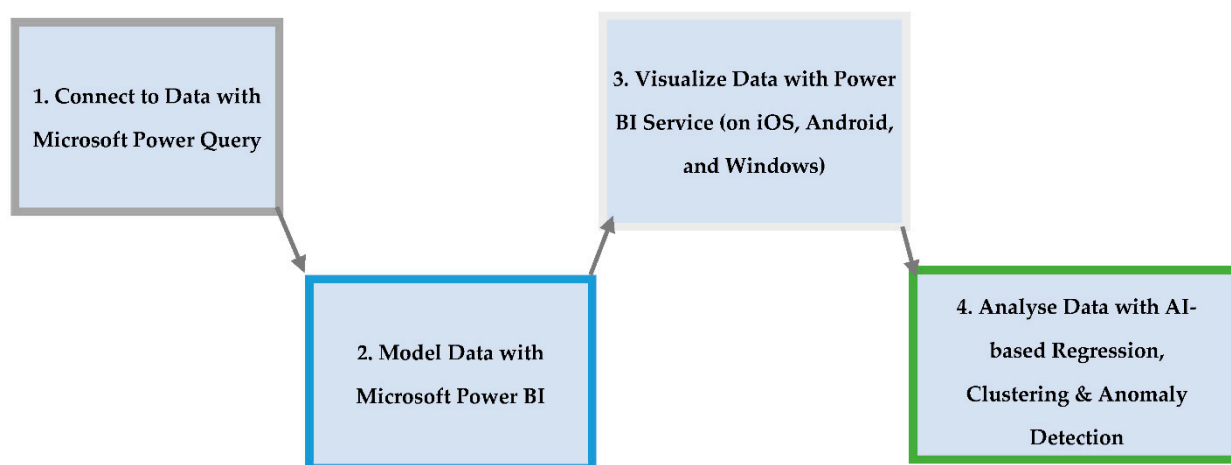


**Figure 1.** High-level methodology of AI insight system for analyzing Australian tropical cyclones.

### 2.1. Data Source

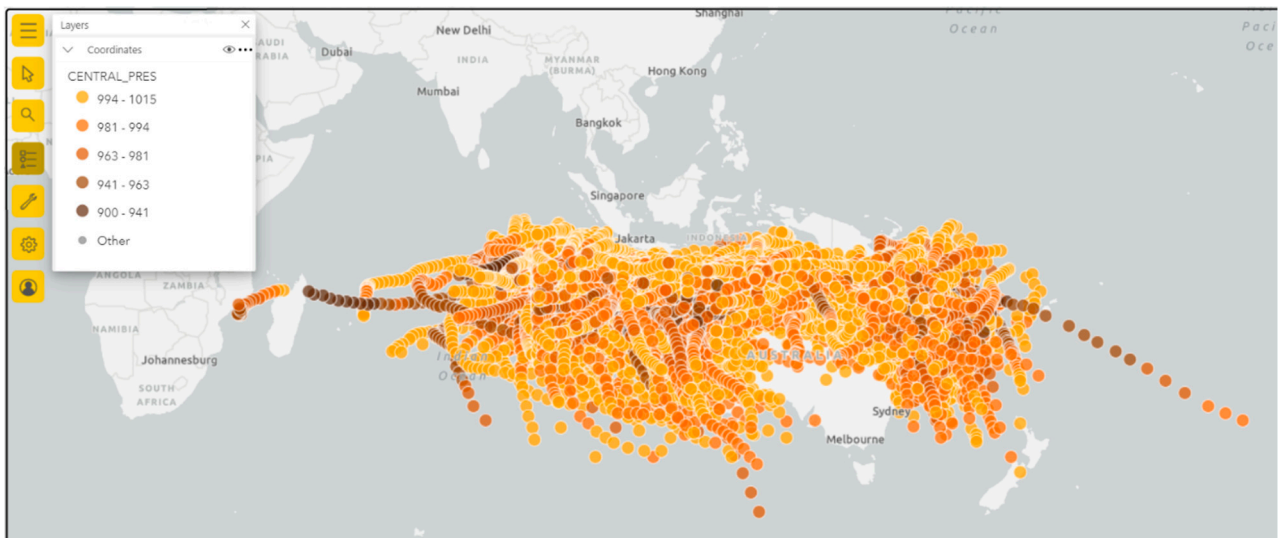
For this study, we used tropical cyclone data captured by the Australian Government's Bureau of Meteorology from 17 January 1907 to 11 May 2022. This captured 1067 Australian cyclones and included 28,713 records with almost 80 cyclone-related parameters. This dataset is available in [13]. The data descriptors and specifications for this massive database is available in [14].

### 2.2. Study Area

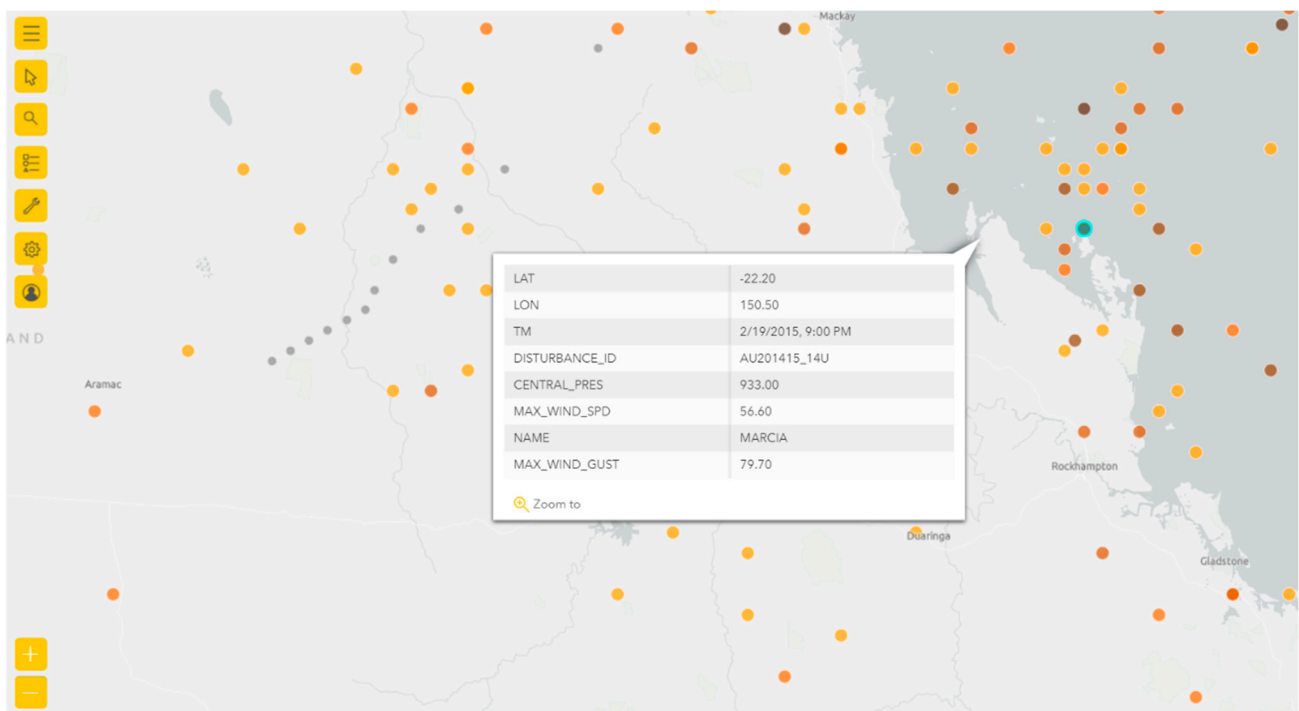
As seen in Figure 2, the study area includes Australia and its surrounding area, with the latitude ranging from  $-48.60$  to  $-2.80$  and the longitude ranging from  $-178.10$  to  $180.00$ . As central pressure and cyclone speed are two of the most important parameters during the categorization of cyclones, one of the critical parameters [16] Figure 2 highlights (i.e., with color codes) is the central pressure. The lower the central pressure of the cyclone, the darker the colors (as shown in the upper left side of Figure 2).

Figure 3 shows Cyclone Marcia that affected Queensland between 15 February and 1 March 2015 and caused about \$587 million of damage. As seen in Figure 3, the selected date point represents the location with latitude  $-22.20$  and longitude  $150.50$  at 9:00 PM on 19 February 2015 with a central pressure of 933 and maximum wind gust of 79.70.

Figure 4 shows one of the most recent cyclones (captured at 6:00 p.m. on 26 February 2022), called Cyclone Anika, while it was located at latitude  $-14.25$  and longitude  $126.70$  with a central pressure of 988 and maximum wind gust of 28.30.



**Figure 2.** Study area within Australia and surrounding area ( $-48.60 < \text{latitude} < -2.80$  and  $-178.10 < \text{longitude} < 180.00$ ).



**Figure 3.** Cyclone Marcia in 2015 located at latitude  $-22.20$  and longitude  $150.50$  (location zoomed). Color code schemes for highlighting the central pressures have been demonstrated previously in Figure 2.

Lastly, a more recent timeline was selected for Figure 5 (date filtered between 26 January 2022 and 11 May 2022); as a result, the paths of the few cyclones that occurred during this time span are displayed. In Figure 5, the specific data point shows Cyclone Charlotte captured at latitude  $-17.05$  and longitude  $109.20$ . The paths of the cyclones are easier to observe in Figure 5 (due to fewer data points) in comparison with Figures 2–4.



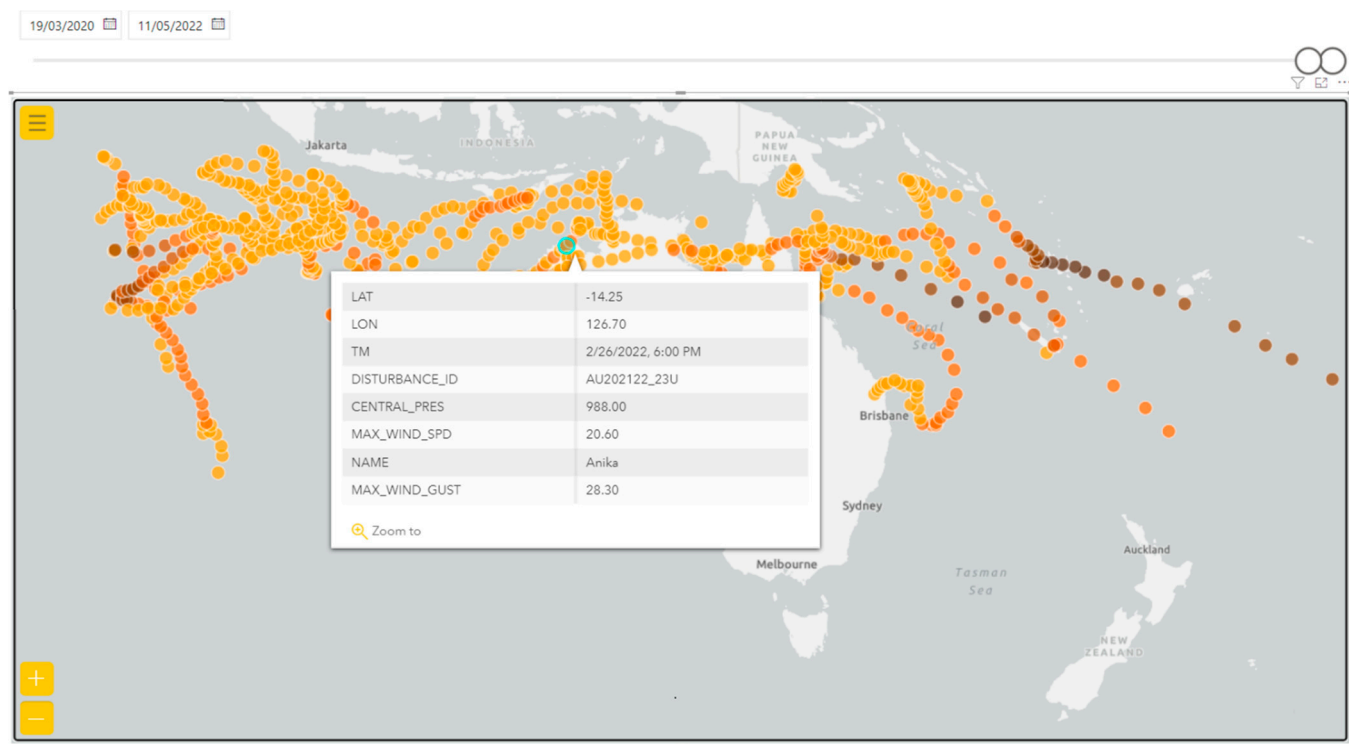


**Figure 4.** Cyclone Anika in 2022 located at latitude  $-14.25$  and longitude  $126.70$  (date filtered between 19 February 2020 and 11 May 2022). Color code schemes for highlighting the central pressures have been demonstrated previously in Figure 2.

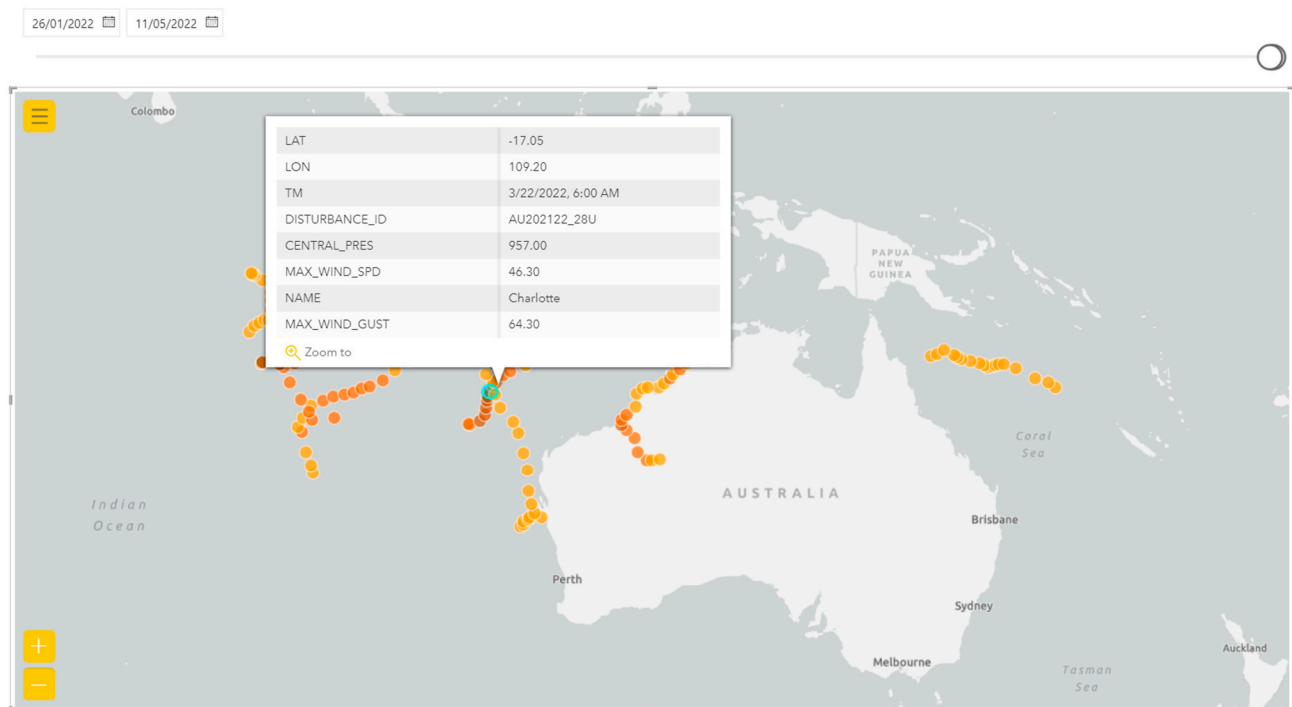


**Figure 5.** Cyclone Anika in 2022 located at latitude  $-17.05$  and longitude  $109.20$  (date filtered between 26 January 2022 and 11 May 2022). Color code schemes for highlighting the central pressures have been demonstrated previously in Figure 2.

### 2.3. Algorithms for Analysis

Selecting the right algorithm to solve the right research question requires a systematic comprehension of the related literature. This study focused on understanding the complex relations among the various parameters related to Australian tropical cyclones to answer several strategic questions, listed in the introduction. To answer questions such as, “What factors influence a cyclone’s central pressure?” or “How do these factors create a cyclone with lower central pressure?”, we used AI-based regression analysis that was depicted in our recent research [6–12,22–24]. To answer strategic questions such as, “What are the characteristics of cyclone events with the lowest central pressure?”, we used k-means clustering with Microsoft Power BI as demonstrated in [12]. Lastly, to effectively answer questions such as, “When did we witness the strongest cyclones with the highest damage potential?” or “What characteristics generate strong cyclones with higher wind speed?”, CNN-based anomaly detection with line chart visualization of Microsoft Power BI was utilized (as demonstrated in our recent studies in [6,7,11,12,22,23]). For this study, we specifically focused on analyzing central pressure and maximum wind speed because of their importance from a meteorological perspective [15,16,25].

#### 2.3.1. Regression

Implementation of a regression analysis automatically ranks the factors that matter, contrasts the relative importance of these factors, and displays them as key influencers for both categorical and numeric metrics. For numerical features, linear regression was performed using SDCA regression implementation from Microsoft’s ML.NET [26]. Linear regression is one of the simplest machine learning algorithms that comes under supervised learning techniques and is used to solve regression problems. It is used to predict the continuous dependent variable with the help of independent variables. The goal of linear regression is to find the = line of best fit that can accurately predict the output for the continuous dependent variable. By finding the line of best fit, the algorithm establishes a linear relationship between the dependent and independent variables in the form of Equation (1).

$$y = b_0 + b_1x_1 + \varepsilon \quad (1)$$

On the other hand, for categorical features, logistic regression was performed using L-BFGS logistic regression from ML.NET [27,28]. Logistic regression is one of the most popular machine learning algorithms that uses supervised learning techniques. It can also be used for classification and regression problems. Logistic regression was used to predict the categorical dependent variable with the help of independent variables using Equation (2).

$$\log[y/y - 1] = b_0 + b_1x_1 + b_2x_2 + \dots b_nx_n \quad (2)$$

The output of the logistic regression problem can only be between zero and one. Logistic regression can be used where the probabilities between two classes are required, such as whether it will rain or not today, 0 or 1, true or false, etc.

Logistic regression without a threshold is a regression. However, by introducing a threshold to the process, it transforms into an efficient classifier. At the beginning, we commence with the logistic or sigmoid function,

$$\sigma(t) = \frac{1}{1 + e^{-t}} \quad (3)$$

which maps real numbers to interval (0, 1). Then, we proceed by defining the hypothesis function with

$$h_{\theta}(x) = \sigma(\theta^T x) = \frac{1}{1 + e^{-\theta^T x}} \quad (4)$$

The classification decision is made on  $y = 1$ , when  $h_\theta(x) \geq 0.5$  and  $y = 0$  otherwise. The decision boundary is  $\theta^T x = 0$ . The cost function is represented by

$$j(\theta) = \sum_{i=1}^m H(y^{(i)}, h_\theta(x^{(i)})) \quad (5)$$

where  $H(p, q)$  is the cross-entropy of distribution  $q$  relative to distribution  $p$  and is given by

$$H(p, q) = - \sum_i p_i \log q_i \quad (6)$$

In this case  $y^{(i)} \in \{0, 1\}$  so  $p_1 = 1$  and  $p_2 = 0$ . Therefore,

$$H(y^{(i)}, h_\theta(x^{(i)})) = -y^{(i)} \log h_\theta(x^{(i)}) - (1 - y^{(i)}) \log(1 - h_\theta(x^{(i)})) \quad (7)$$

Similar to the selection of the quadratic cost function in linear regression, the selection of this cost function is mainly driven by the fact that it is efficient and easy to implement, as shown in

$$\text{grad } J(\theta) = \frac{\partial J(\theta)}{\partial \theta} = \begin{bmatrix} \frac{\partial}{\partial \theta_0} J(\theta) \\ \frac{\partial}{\partial \theta_1} J(\theta) \\ \vdots \\ \frac{\partial}{\partial \theta_n} J(\theta) \end{bmatrix} = X^T (h_\theta(X) - y) \quad (8)$$

Hence, gradient descent for logistic regression could be reflected with

$$\theta(k+1) = \theta(k) - s \text{grad } J(\theta) \quad (9)$$

### 2.3.2. K-Means Clustering

Our implementation of k-means clustering is based on automated AI-based clustering algorithms of Microsoft Power BI [21]. The k-means algorithm in this study used data pertaining to Australian tropical cyclone events to analyze almost 80 parameters. Assuming we have input data points  $x_1, x_2, x_3, x_4, \dots, x_n$ , the k-means clustering algorithm randomly selects  $k$  points as the initial centroid from the dataset. Then, Euclidian distances are calculated for each point in the dataset with respect to the selected  $k$  points, known as cluster centroids. Given for two points,  $p = (p_1, p_2)$  and  $q = (q_1, q_2)$ , and the Euclidian distance is measured with Equation (10).

$$d(p, q) = \sqrt{(q_1 - p_1)^2 + (q_2 - p_2)^2} \quad (10)$$

After finding the Euclidean distances of each point with the cluster centroids, each data point is assigned to the cluster centroid for which the distance is minimal, as seen in Equation (11).

$$\underset{c_i \in C}{\text{argmin}} \text{dist}(c_i, x)^2 \quad (11)$$

Here,  $\text{dist}()$  is the Euclidean distance. Next, the new centroid is calculated by taking the average of the points in each cluster group, as seen in Equation (12).

$$c_i = \frac{1}{|S_i|} \sum_{x_i \in S_i} x_i \quad (12)$$

Here,  $S_i$  is the set of all points assigned to the  $i$ th cluster. This process of calculating the Euclidian distances (with Equation (10)), assigning points to the cluster centroid (with Equation (11)), and finding the new centroid by taking the average (with Equation (12)) is continued for several iterations until the centroids do not change. At the end of these

iterations,  $k$  numbers of cluster centroids are discovered, and data points are assigned to the right clusters. It should be mentioned that the implementation in Microsoft Power BI obviated the requirements for manually selecting the  $k$  number (or the number of clusters). Moreover, AI-based automated clustering by Microsoft Power BI eliminates the requirement of manual preprocessing (e.g., normalization, data transformation, etc.) of input data.

### 2.3.3. CNN-Based Anomaly Detection

The anomaly detector enhances line charts by automatically detecting anomalies within time-series data. It also provides explanations for the anomalies to facilitate root-cause analysis. In our most recent study, we harnessed the anomaly detection algorithm to identify abnormal cases of landslides and obtain the root causes of these anomalies [6,7]. Moreover, we recognized and explained the anomalies for disaster events using anomaly detection in social media [11,12]. Furthermore, we have classified anomalies on global events by monitoring 2397 global news sources and applying anomaly detection algorithms [22,23]. Before delving into the details of anomaly detection, we present the problem definition.

**Problem 1:** Given a sequence of real values, that is,  $x = x_1, x_2, x_3, \dots, x_n$ , the task of time-series anomaly detection is to produce an output sequence  $y = y_1, y_2, y_3, \dots, y_n$ , where  $y_i \in \{0, 1\}$  denotes whether  $x_i$  is an anomaly point.

The implemented solution borrowed the SR from the visual saliency detection domain and then applied a CNN to the results produced by the SR model [29].

The SR algorithm consists of three major steps:

- Perform Fourier transform to obtain the log amplitude spectrum.
- Calculate the SR.
- Perform inverse Fourier transform, which transforms the sequence back to the spatial domain.

$$A(f) = \text{Amplitude}(f(x)) \quad (13)$$

$$P(f) = \text{Phase}(f(x)) \quad (14)$$

$$L(f) = \log(A(f)) \quad (15)$$

$$AL(f) = h_q(f) \cdot L(f) \quad (16)$$

$$R(f) = L(f) - AL(f) \quad (17)$$

$$S(x) = \left\| f^{-1}(\exp(R(f) + iP(f))) \right\| \quad (18)$$

where  $f$  and  $f^{-1}$  denote the Fourier transform and inverse Fourier transform, respectively;  $x$  is the input sequence with shape  $n \times 1$ ;  $A(f)$  is the amplitude spectrum of sequence  $x$ ;  $P(f)$  is the corresponding phase spectrum of sequence  $x$ ;  $L(f)$  is the log representation of  $A(f)$ ; and  $AL(f)$  is the average spectrum of  $L(f)$ , which can be approximated by convoluting the input sequence by  $h_q(f)$ , where  $h_q(f)$  is a  $q \times q$  matrix defined as:

$$h_q(f) = \frac{1}{q^2} \begin{bmatrix} 1 & 1 & \dots & 1 \\ 1 & 1 & \dots & 1 \\ \dots & \vdots & \ddots & \vdots \\ 1 & 1 & \dots & 1 \end{bmatrix} \quad (19)$$

$R(f)$  is the SR, that is, the log spectrum  $L(f)$  minus the averaged log spectrum  $AL(f)$ . The SR serves as a compressed representation of the sequence, whereas the innovation part of the original sequence becomes more significant. Last, the sequence was transferred back to the spatial domain using an inverse Fourier transform. The resultant sequence  $S(x)$

is referred to as the saliency map [30]. The values of the anomaly points are calculated as follows:

$$x = (\bar{x} + \text{mean})(1 + \text{var}) \cdot r + x \quad (20)$$

where  $\bar{x}$  is the local average of the preceding points, mean and var are the mean and variance of all points within the current sliding window, and  $r \sim N(0, 1)$  is randomly sampled. In this process, CNN is applied to the saliency map instead of to the raw input, increasing the efficiency of the overall process of anomaly detection [29,30].

The anomaly detection algorithm provides detailed explanations for all detected anomalies following the root cause analysis performed by AI services. We implement anomaly detection in three steps:

- Detect all the anomalies within the time series (i.e., any values that lie outside the threshold range).
- Identify the main drivers of these anomalies.
- Explain the results in a natural language (explanation of the root cause) using NLP [31].

### 3. Results

Our study allows disaster strategists, planners, and researchers to answer the “What”, “When”, “How”, and “Why” questions on central pressure and maximum cyclone speed of Australian tropical cyclones by using an interactive dashboard that was developed during the course of this research. There were three distinct types of functionalities satisfied by three distinct types of AI-based algorithms (e.g., regression, clustering, and deep learning). This section briefly discusses the results obtained from utilizing these three different types of algorithms.

#### 3.1. Results on Regression

Regression analysis answered the following questions, among others:

- What factors influence a cyclone’s central pressure?
- How do these factors create a cyclone with lower central pressure?
- Explain why.

As seen in Figure 6, we used the key influencers visual from Microsoft Power BI to identify all the factors that influence the central pressure of Australian tropical cyclones, as central pressure is one of the key elements that determines the damage potential of a cyclone. By employing automated regression analysis (i.e., both linear and logistic regression) on almost 80 cyclone-related factors, our solution found 33 factors that directly influence the central pressure of Australian tropical cyclones (as seen in Figure 6 and Table 1). The descriptions, data types, and units of these 80 cyclone-related parameters can be found at [14]. Among these relationships, items number 21 and 33 from Table 1 depicts results from the linear regression on numerical variables (i.e., maximum wind speed, maximum wind gust, etc.). For the case item 21 from Table 1, the relationship between maximum wind speed and central pressure was explained by NLP as, “When Maximum wind speed goes up 11.71 is more than 167, the average of Central Pressure decreases by 11.48”. On the other hand, for item 33 from Table 1, the relationship between maximum wind gust and central pressure was explained by our system as, “When Maximum wind gust goes down 14.98, the average of Central Pressure decreases by 0.61” (as shown in Figure 7). Whereas Figure 6 demonstrates a case logistic regression, Figure 7 represents a case for linear regression. It should be noted that with the help of regression analysis and NLP on almost 80 factors, we successfully explained the 33 identified relationships (as shown in Table 1). Previous studies in [8,9,15–18] have not reported such a comprehensive level of analysis (i.e., analyzing 80 cyclone parameters to understand the intricate relationships among them).



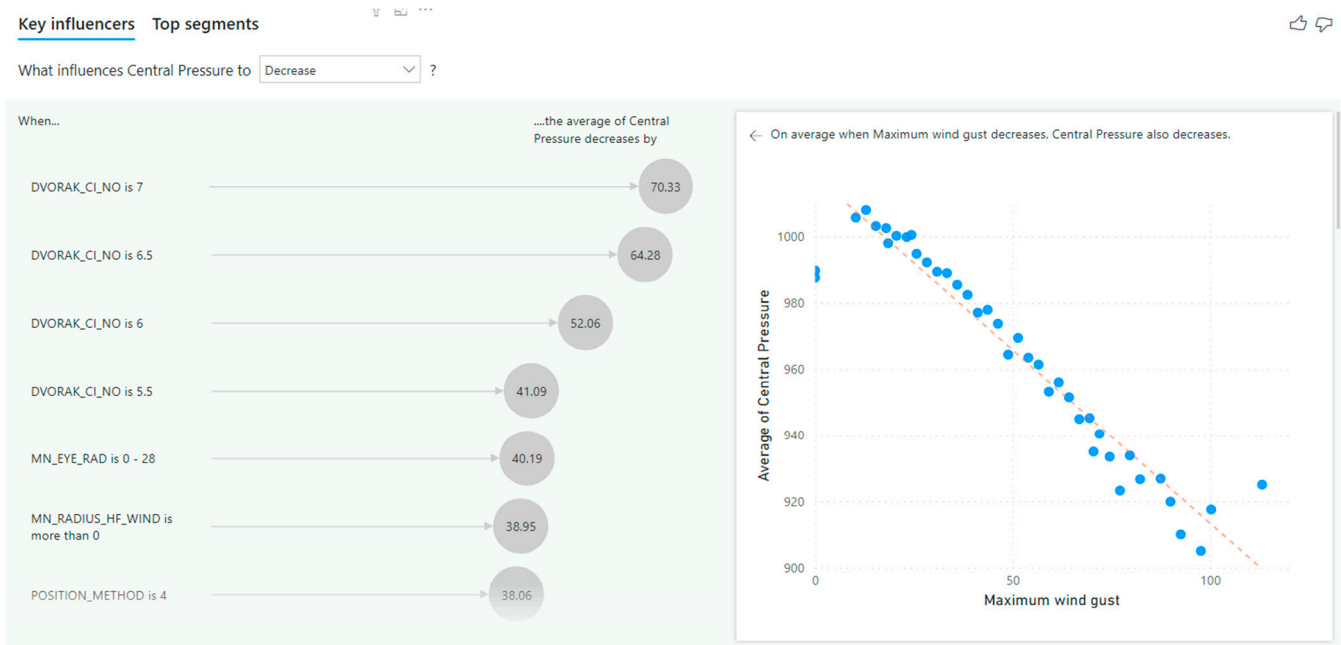


**Figure 6.** Key influencers visualization from Microsoft Power BI identified and explained all factors influencing central pressure of Australian tropical cyclones.

**Table 1.** 33 factors that influence the central pressure of cyclones with NLP-based descriptions (specifications of these factors are available at [14]). There is no copyright issue, as all the pictures and associated descriptions were generated using the presented solution.

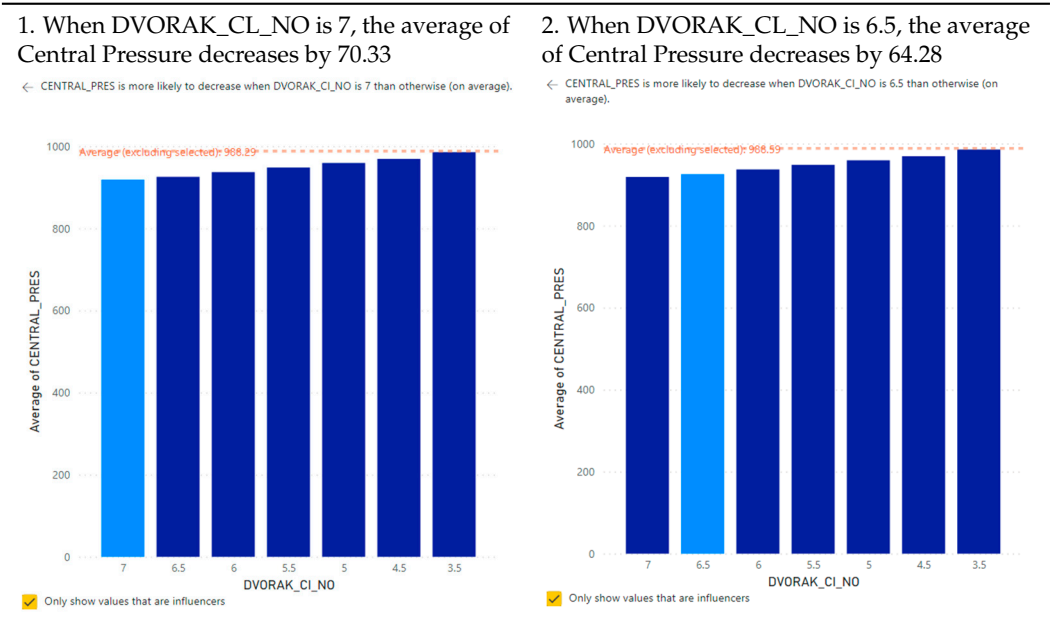
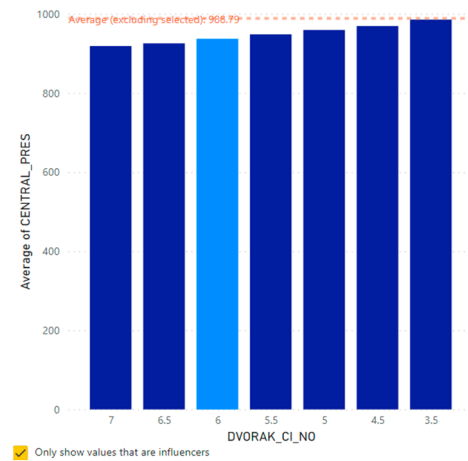


Table 1. Cont.

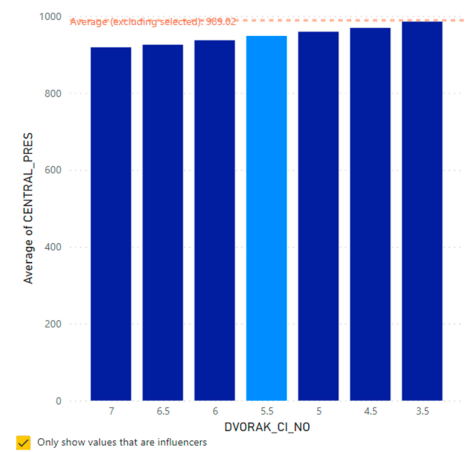
3. When DVORAK\_CL\_NO is 6, the average of Central Pressure decreases by 52.06

← CENTRAL\_PRES is more likely to decrease when DVORAK\_CL\_NO is 6 than otherwise (on average).



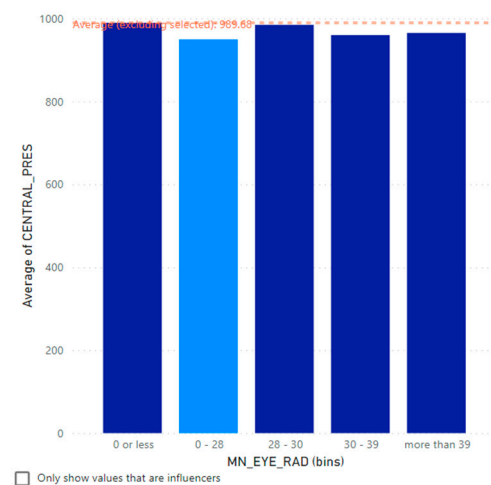
4. When DVORAK\_CL\_NO is 5.5, the average of Central Pressure decreases by 41.09

← CENTRAL\_PRES is more likely to decrease when DVORAK\_CL\_NO is 5.5 than otherwise (on average).



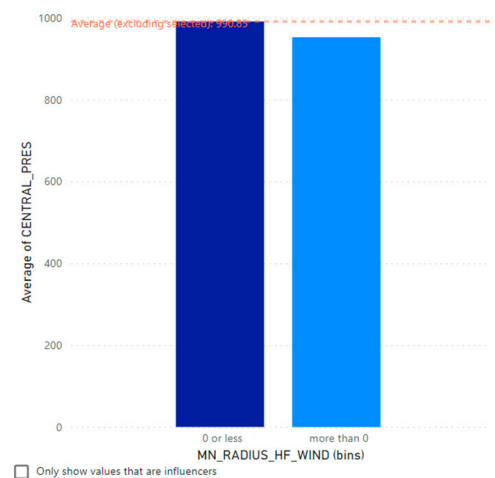
5. When MN\_EYE\_RAD is 0–28, the average of Central Pressure decreases by 40.19

← CENTRAL\_PRES is more likely to decrease when MN\_EYE\_RAD is 0–28 than otherwise (on average).



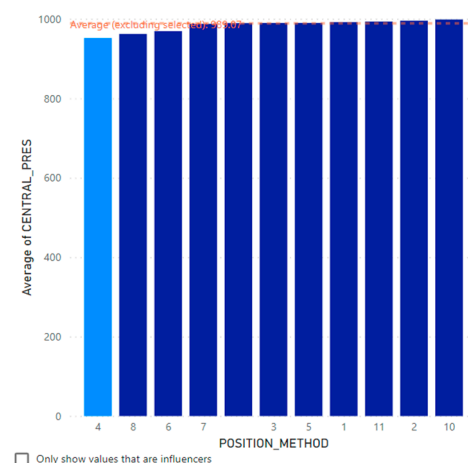
6. When MN\_RADIUS\_HF\_WIND is more than 0, the average of Central Pressure decreases by 38.95

← CENTRAL\_PRES is more likely to decrease when MN\_RADIUS\_HF\_WIND is more than 0 than otherwise (on average).



7. When POSITION\_METHOD is 4, the average of Central Pressure decreases by 38.06

← CENTRAL\_PRES is more likely to decrease when POSITION\_METHOD is 4 than otherwise (on average).



8. When CYC\_TYPE is 40, the average of Central Pressure decreases by 38.03

← CENTRAL\_PRES is more likely to decrease when CYC\_TYPE is 40 than otherwise (on average).

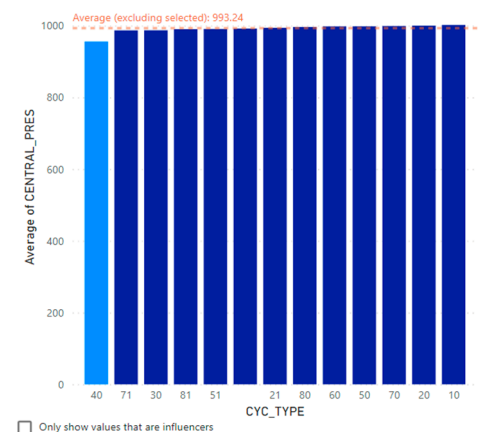
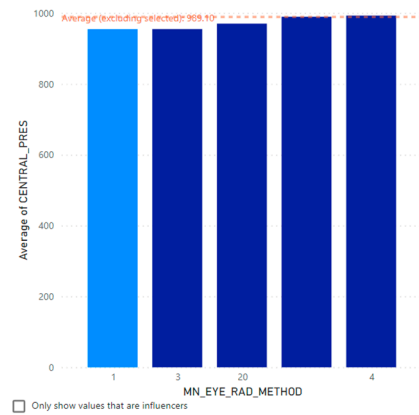


Table 1. Cont.

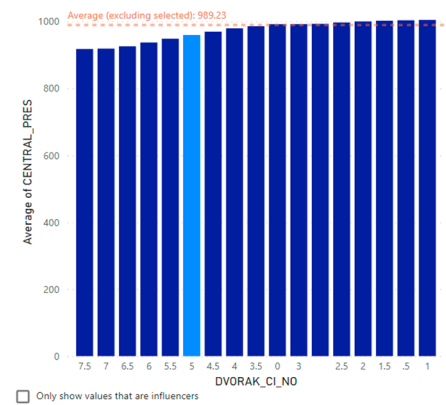
9. When MN\_EYE\_RAD\_METHOD is 1, the average of Central Pressure decreases by 34.46

← CENTRAL\_PRES is more likely to decrease when MN\_EYE\_RAD\_METHOD is 1 than otherwise (on average).



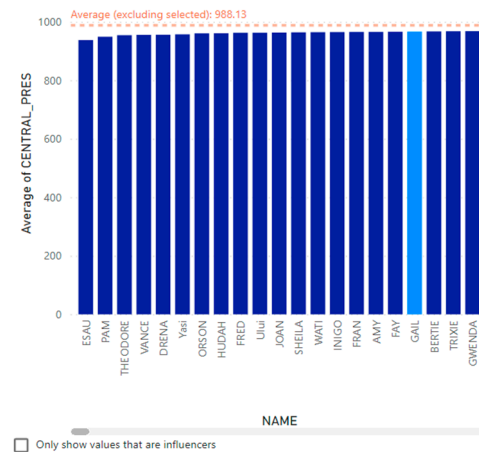
10. When DVORAK\_CL\_NO is 5, the average of Central Pressure decreases by 30.16

← CENTRAL\_PRES is more likely to decrease when DVORAK\_CL\_NO is 5 than otherwise (on average).



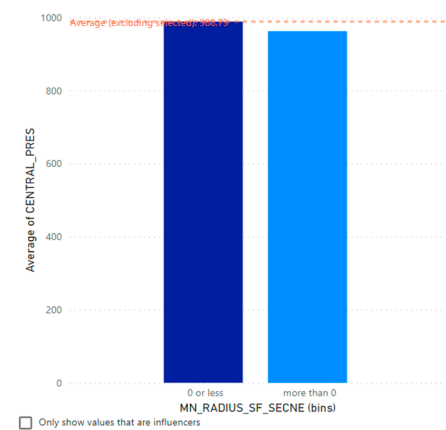
11. When Name is GAIL, the average of Central Pressure decreases by 27.02

← CENTRAL\_PRES is more likely to decrease when NAME is GAIL than otherwise (on average).



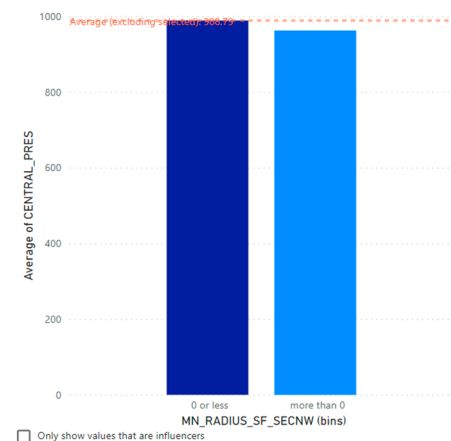
12. When MN\_RADIUS\_SF\_SECNE is more than 0, the average of Central Pressure decreases by 26.95

← CENTRAL\_PRES is more likely to decrease when MN\_RADIUS\_SF\_SECNE is more than 0 than otherwise (on average).



13. When MN\_RADIUS\_SF\_SECNW is more than 0, the average of Central Pressure decreases by 26.94

← CENTRAL\_PRES is more likely to decrease when MN\_RADIUS\_SF\_SECNW is more than 0 than otherwise (on average).



14. When MN\_RADIUS\_GF\_WIND is more than 111, the average of Central Pressure decreases by 23.36

← CENTRAL\_PRES is more likely to decrease when MN\_RADIUS\_GF\_WIND is more than 111 than otherwise (on average).

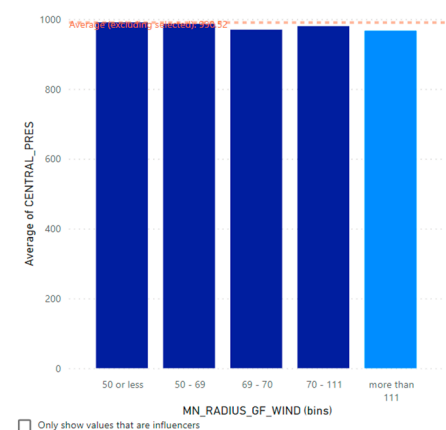
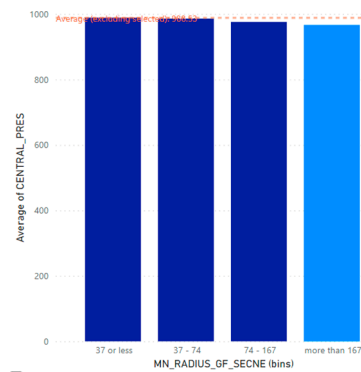


Table 1. Cont.

15. When MN\_RADIUS\_SECNE is more than 167, the average of Central Pressure decreases by 23.06

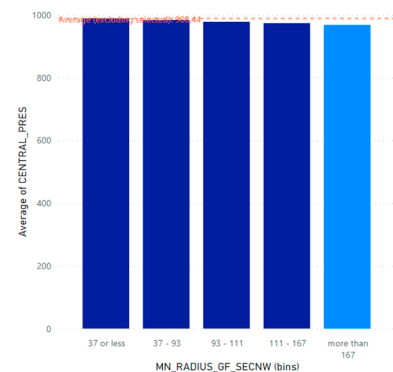
← CENTRAL\_PRES is more likely to decrease when MN\_RADIUS\_GF\_SECNE is more than 167 than otherwise (on average).



☐ Only show values that are influencers

16. When MN\_RADIUS\_SECNW is more than 167, the average of Central Pressure decreases by 21.72

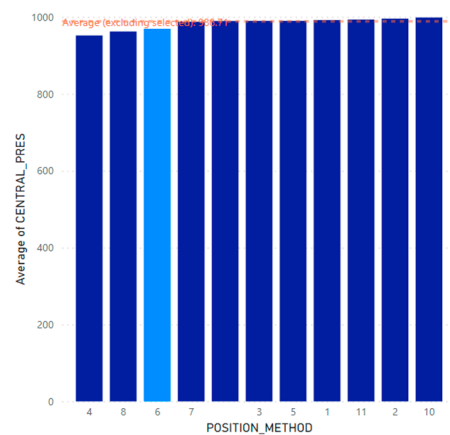
← CENTRAL\_PRES is more likely to decrease when MN\_RADIUS\_GF\_SECNW is more than 167 than otherwise (on average).



☐ Only show values that are influencers

17. When POSITION\_METHOD 6, the average of Central Pressure decreases by 20.78

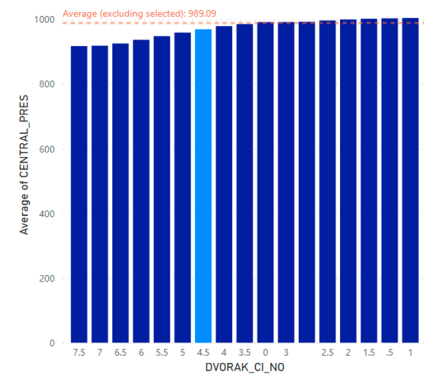
← CENTRAL\_PRES is more likely to decrease when POSITION\_METHOD is 6 than otherwise (on average).



☐ Only show values that are influencers

18. When DVORAK\_CL\_NO is 4.5 is more than 167, the average of Central Pressure decreases by 20.17

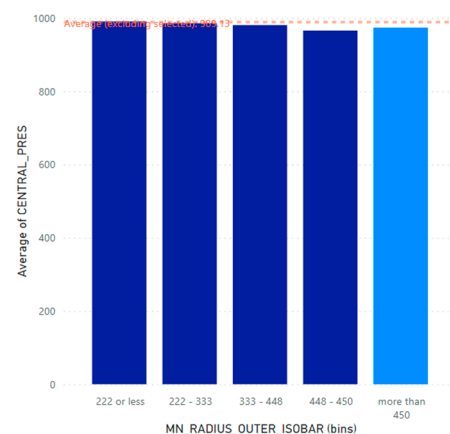
← CENTRAL\_PRES is more likely to decrease when DVORAK\_CL\_NO is 4.5 than otherwise (on average).



☐ Only show values that are influencers

19. When MN\_RADIUS\_OUTER\_ISOBA... is more than 450, the average of Central Pressure decreases by 15.08

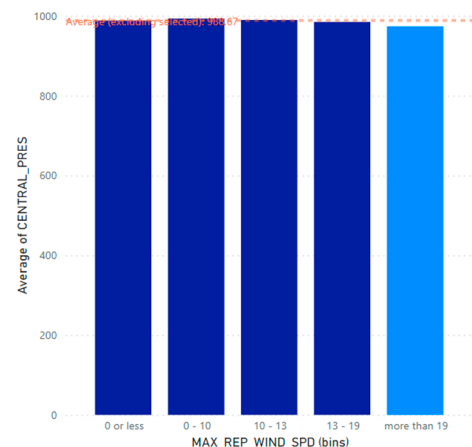
← CENTRAL\_PRES is more likely to decrease when MN\_RADIUS\_OUTER\_ISOBA... is more than 450 than otherwise (on average).



☐ Only show values that are influencers

20. When MAX\_REP\_WIND\_SPD is more than 19, the average of Central Pressure decreases by 13.89

← CENTRAL\_PRES is more likely to decrease when MAX\_REP\_WIND\_SPD is more than 19 than otherwise (on average).

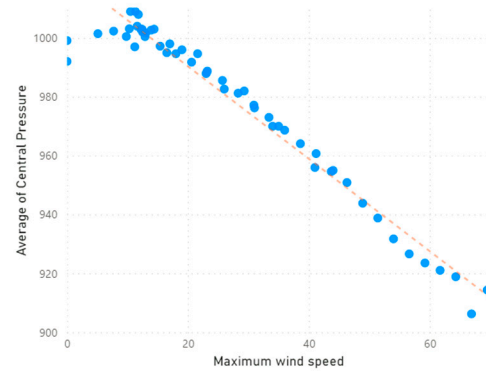


☐ Only show values that are influencers

Table 1. Cont.

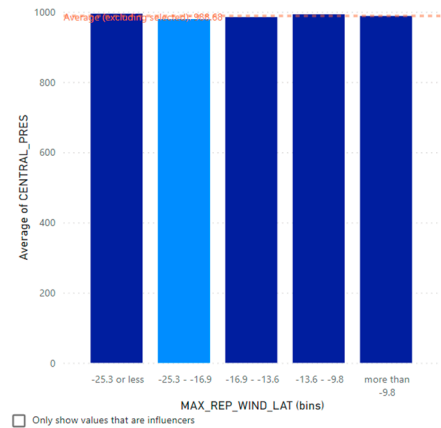
21. When Maximum wind speed goes up 11.71 is more than 167, the average of Central Pressure decreases by 11.48

← On average when Maximum wind speed increases, Central Pressure decreases.



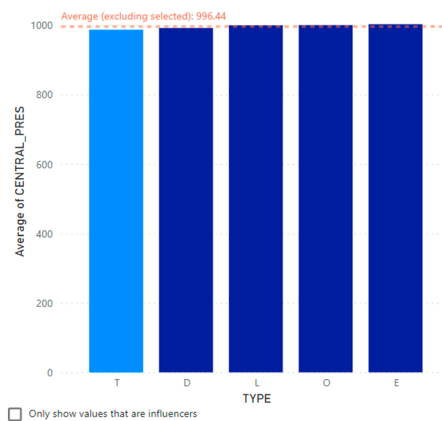
22. When MAX\_REP\_WIND\_LAT is between −25.3 and −16.9, the average of Central Pressure decreases by 9.74

← CENTRAL\_PRES is more likely to decrease when MAX\_REP\_WIND\_LAT is −25.3 - −16.9 than otherwise (on average).



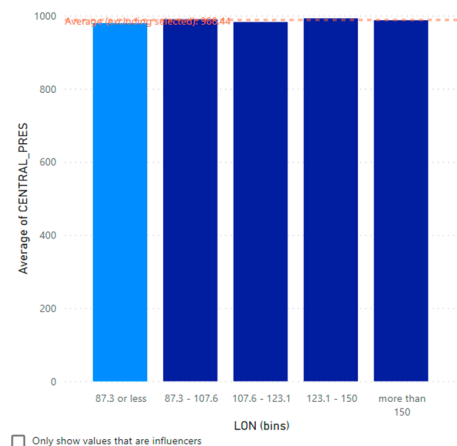
23. When TYPE is T, the average of Central Pressure decreases by 9.5

← CENTRAL\_PRES is more likely to decrease when TYPE is T than otherwise (on average).



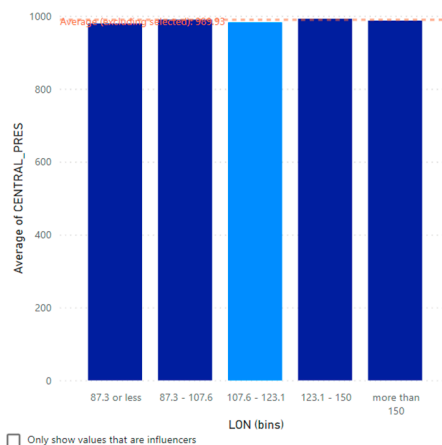
24. When LON is less 87.3 or less, the average of Central Pressure decreases by 9.07

← CENTRAL\_PRES is more likely to decrease when LON is 87.3 or less than otherwise (on average).



25. When LON is between 107.6 and 123.1, the average of Central Pressure decreases by 7.77

← CENTRAL\_PRES is more likely to decrease when LON is 107.6 - 123.1 than otherwise (on average).



26. When LAT is between −26.2 and −17.3, the average of Central Pressure decreases by 7.53

← CENTRAL\_PRES is more likely to decrease when LAT is −26.2 - −17.3 than otherwise (on average).

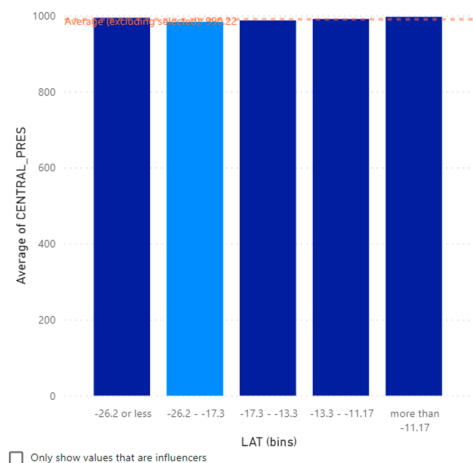
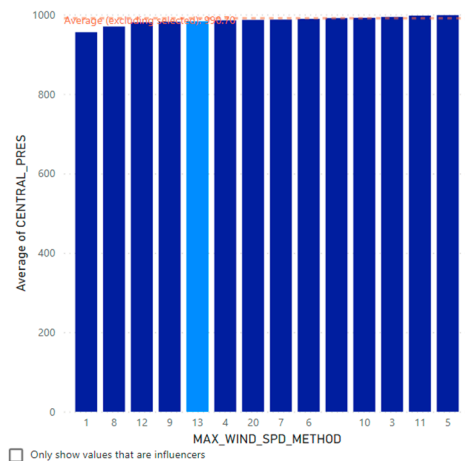




Table 1. Cont.

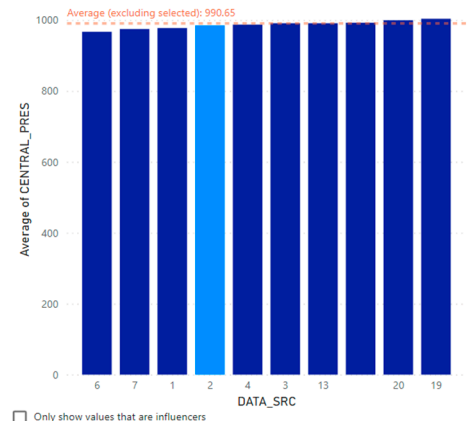
27. When MAX\_WIND\_SPD\_METHOD is 13, the average of Central Pressure decreases by 7.4

← CENTRAL\_PRES is more likely to decrease when MAX\_WIND\_SPD\_METHOD is 13 than otherwise (on average).



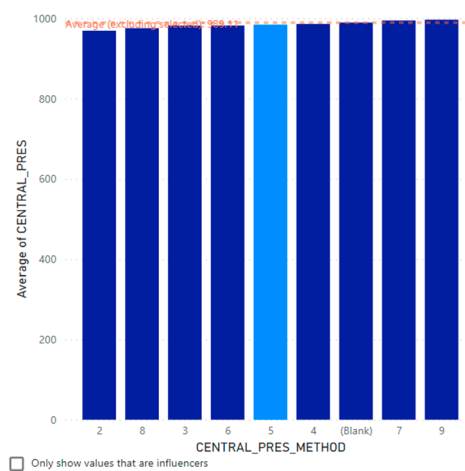
28. When DATA\_SRC is 2, the average of Central Pressure decreases by 5.89

← CENTRAL\_PRES is more likely to decrease when DATA\_SRC is 2 than otherwise (on average).



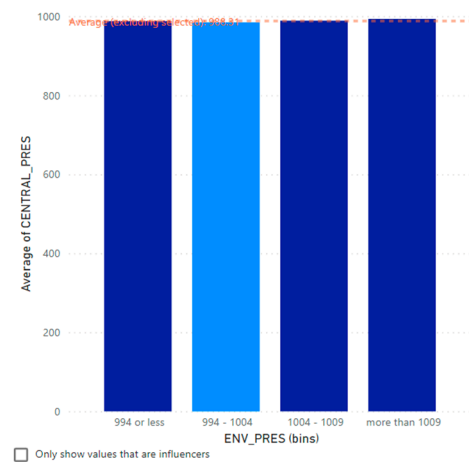
29. When CENTRAL\_PRES\_METHOD is 5, the average of Central Pressure decreases by 5.28

← CENTRAL\_PRES is more likely to decrease when CENTRAL\_PRES\_METHOD is 5 than otherwise (on average).



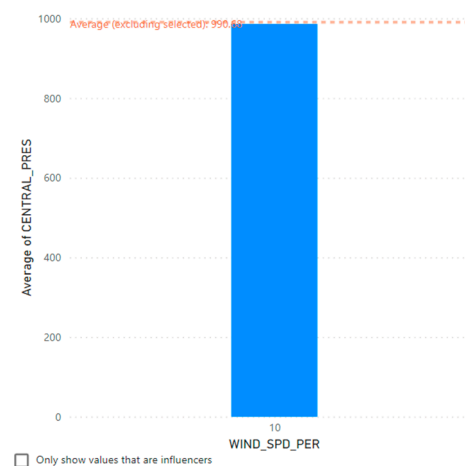
30. When ENV\_PRES is between 994 and 1004, the average of Central Pressure decreases by 4.9

← CENTRAL\_PRES is more likely to decrease when ENV\_PRES is 994 - 1004 than otherwise (on average).



31. When WIND\_SPD\_PER is 10, the average of Central Pressure decreases by 4.57

← CENTRAL\_PRES is more likely to decrease when WIND\_SPD\_PER is 10 than otherwise (on average).



32. When DVORAK\_CI\_NO is 3.5, the average of Central Pressure decreases by 2.64

← CENTRAL\_PRES is more likely to decrease when DVORAK\_CI\_NO is 3.5 than otherwise (on average).

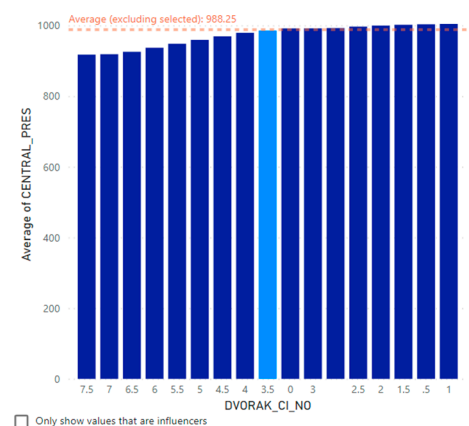
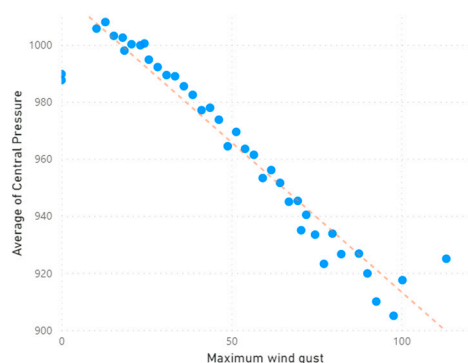


Table 1. Cont.

33. When MAX\_WIND\_GUST goes down 14.98, the average of Central Pressure decreases by 0.61

← On average when Maximum wind gust decreases, Central Pressure also decreases.



#### Key influencers Top segments

What influences Central Pressure to  ?

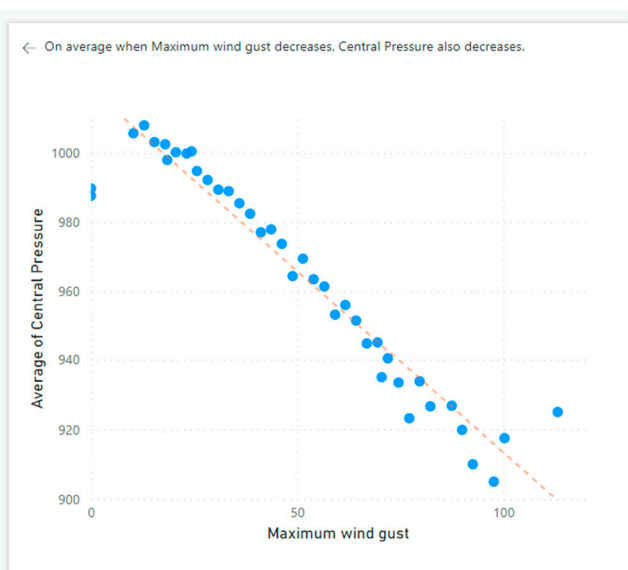


**Figure 7.** Linear regression showing the linear relationship between numerical variable MAX\_WIND\_GUST and Central Pressure.

### 3.2. Results on Clustering

We used k-means clustering to answer strategic questions such as, “How can we identify the characteristics of cyclone events with the lowest central pressure?” or “What are the conditions for a cyclone with low central pressure?”. Key influencers visual from Microsoft Power BI was used to perform automated k-means clustering where the number of clusters were automatically determined by our solution. As seen in Figure 8, four clusters or segments were discovered for analyzing cyclones with low pressure. The average central pressure for segments 1, 2, 3, and 4 were 939.5, 964.9, 979.5, and 986.7 hPa, respectively. Clicking each of these identified segments reveal their characteristics, as shown in Figure 9. As seen in Figure 9, the key characteristic of Segment 1 with the lowest central pressure was “Maximum wind speed is more than 44”. Table 2 demonstrates the detailed characteristics discovered by the clustering analysis for all four segments.



**Figure 8.** Clustering analysis automatically discovered four segments for answering questions such as, “When is central pressure more likely to be low”.

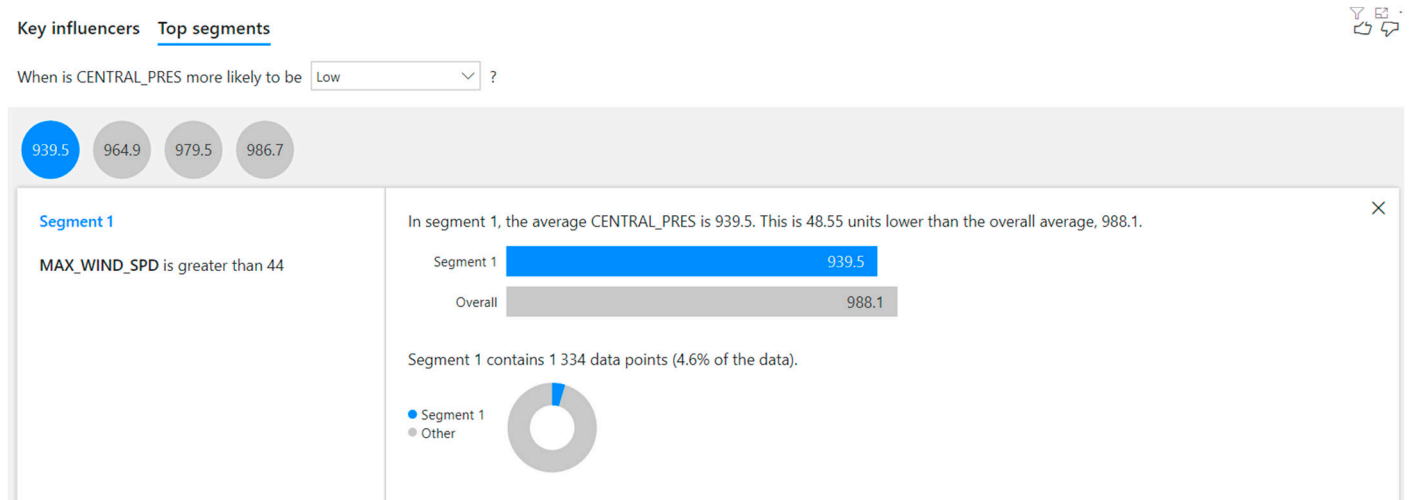


**Figure 9.** Characteristics of Segment 1 with average central pressure of 939.5 hPa.

**Table 2.** Characteristics discovered by k-means clustering for all four segments.

Segment No.	Central Air Pressure (hPa)	Data Points Analyzed	Characteristics Discovered by Clustering
1	939.5	1334	44 < Maximum wind speed
2	964.9	2495	31 < Maximum wind speed ≤ 44
3	979.5	1789	25.7 < Maximum wind speed ≤ 31
4	986.7	2715	21.6 < Maximum wind speed ≤ 25.7

### 3.3. Results on Anomaly Detection

We used CNN-based anomaly detection to detect anomalies in the time series record of Australian tropical cyclones. By using the analytical features of line chart visualization in Microsoft Power BI, we answered the following strategic questions, among others:

- When did we witness the strongest cyclones with the highest damage potential?
- What characteristics generate strong cyclones with higher wind speeds?
- Explain why.

As shown in Figure 10, 22 anomalies were automatically detected and highlighted by our solution, at 70% sensitivity. Clicking any one of these anomalies launches our implementation of the CNN algorithm to find out the root causes of the selected anomaly. As shown in Figure 11, the identified root causes are explained in plain language with the help of NLP. First, Figure 11a explains why the selected anomaly was identified as an anomaly (i.e., being outside of tolerance levels). Then, Figure 11b,c explains two possible root causes out of five total root causes for the selected month (i.e., March 2004). CNN-based deep learning or anomaly detection found that, in March 2004, the aggregated wind-speed (5273.80 km/h) of all cyclones were more than the expected range from 1179.49 to 1755.39 km/h. The algorithm highlights this month to be an anomaly and proceeds to explain the root causes with corresponding confidence strengths.

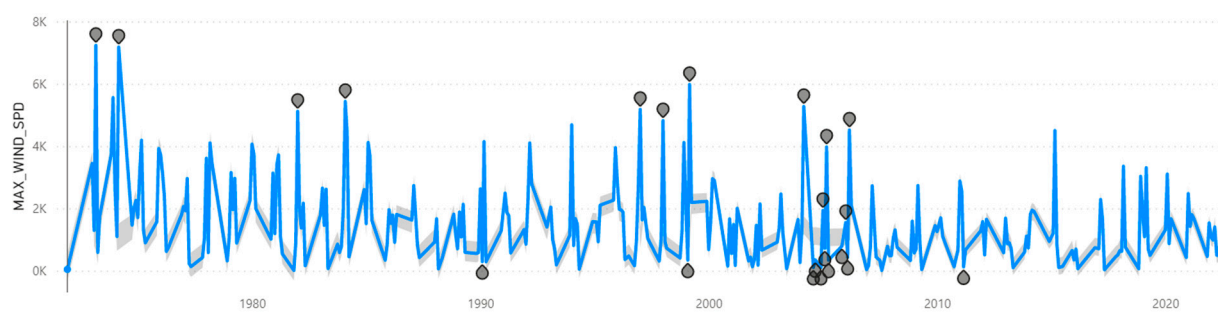


Figure 10. Anomalies detected and highlighted on cyclones with abnormally higher or lower speeds.

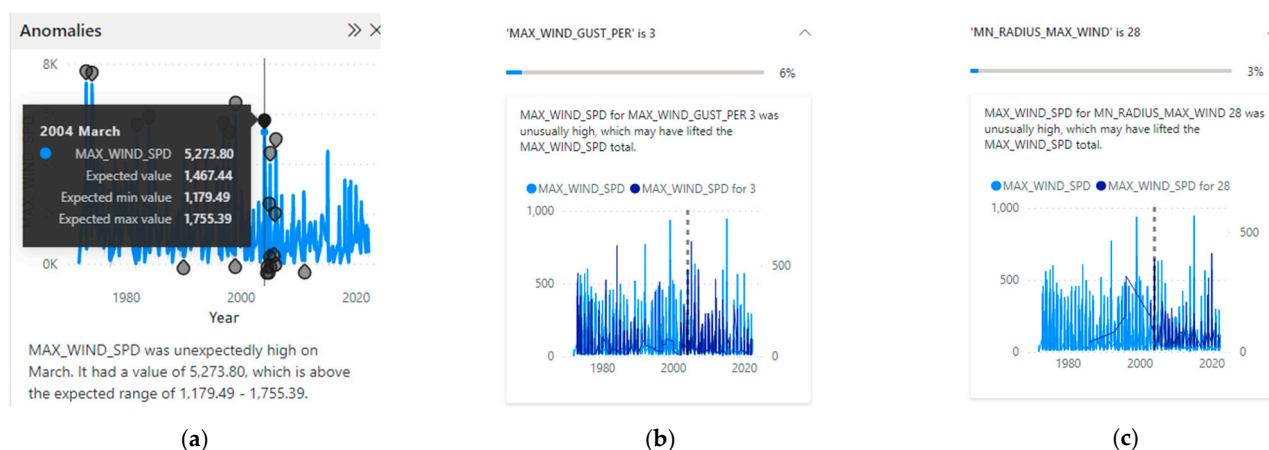


Figure 11. Root causes of selected anomaly described in plain language.

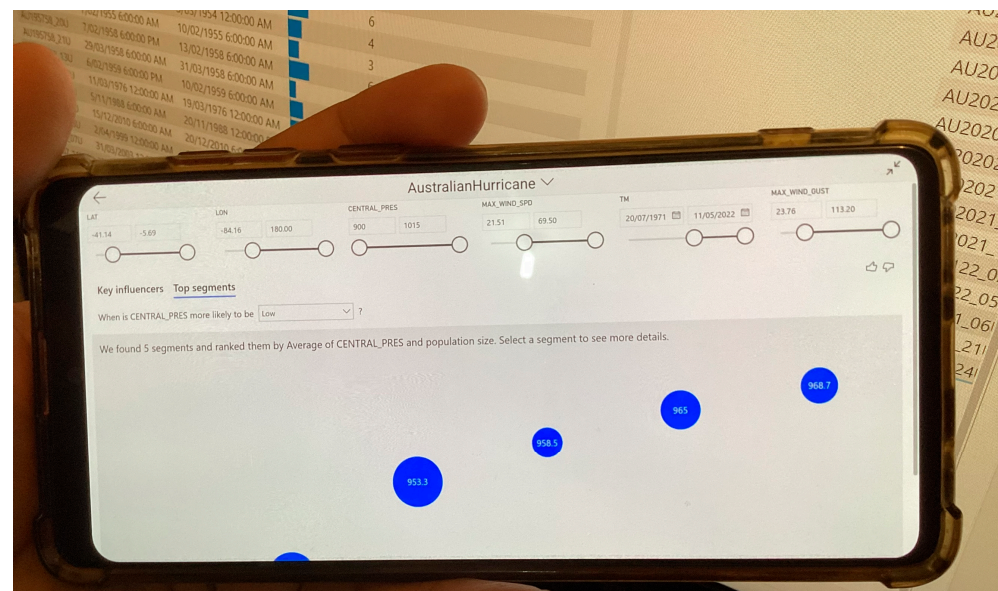
It should be noted that the anomalies highlighted in Figure 10 were at 70% sensitivity of the deployed CNN algorithm. Increasing the sensitivity of the CNN algorithm allows our deployed solution to identify and explain more anomalies. Table 3 shows the detailed results on the number of anomalies identified on varying sensitivity scales.

**Table 3.** Number of anomalies detected at different sensitivities of CNN-based anomaly detection.

Sensitivity of Anomaly Detection	Number of Detected Anomalies
65%	17
70%	22
75%	22
80%	22
85%	31
90%	31
95%	90
100%	90

#### 4. Discussion

The results depicted in Figures 6–11 and Tables 1–3 were obtained based on a full range of dates, latitudes, longitudes, wind gusts, wind speeds, and central pressure. However, our interactive system allows strategic decision-makers to quickly create a scenario by adjusting several of these cyclone parameters (i.e., dates, latitude, longitude, wind gust, wind speed, and central pressure). For example, Figure 12 depicts a user only interested in latitudes between  $-41.14$  and  $-5.69$ , longitudes between  $-84.16$  and  $180.00$ , central pressures between  $900$  and  $1015$ , maximum wind speeds between  $21.51$  and  $69.50$ , and dates between  $20$  July  $1971$  and  $11$  May  $2022$ . Based on these cyclone-related parameters, all cyclone events fulfilling the user's conditions were selected and the clustering algorithm was run on these selected records. The results of the clustering algorithm are different to what was observed in Figures 8 and 9. Thus, the presented solution supports an exhaustive range of scenarios, where the user of the system specifies a range of conditions and AI algorithms are only applied on the records satisfying the user's specifications.

**Figure 12.** Automated clustering running on an Android app on Samsung Galaxy Note 10 Lite smartphone.

To calculate the number of scenarios, we first need to calculate the possible options for each of the features. For example, a cyclone parameter called cyclone-type may contain only three values such as *Low*, *Medium*, and *Extreme*. Therefore, it could have the following filter options:



- {Low}
- {Medium}
- {Extreme}
- {Low, Medium}
- {Low, Extreme}
- {Medium, Extreme}
- {Low, Medium, Extreme}

Thus, for the cyclone-type parameter, there are seven possible filter settings as represented by  $(2^{|N|} - 1)$ , which is the formula to calculate the power set of type attribute minus 1 (i.e.,  $P(N) - 1$ ). Here,  $|N|$  is the cardinality of set cyclone-type. We deduct one because the power set also includes an empty set and the selection of an empty set is not supported by the system.

Hence, the total number of scenarios could be calculated as

$$|S| = (2^{|a|} - 1) \times (2^{|b|} - 1) \times (2^{|c|} - 1) \times (2^{|d|} - 1) \times (2^{|e|} - 1) \times (2^{|f|} - 1) \quad (21)$$

Within Equation (21),  $a$  is the cardinality of latitude,  $b$  is the cardinality of longitude,  $c$  is the cardinality of central pressure,  $d$  is the cardinality of maximum wind speed,  $e$  is the cardinality of dates, and  $f$  is the cardinality of maximum wind gust. If we apply Equation (21) on our deployed solution, as shown in Figure 12, we obtain  $4.737 \times 10^{8234}$  scenarios. The number of scenarios would increase if we incorporated more cyclone parameters. The purpose of this section is not only to produce an exhaustive list of insights from the Australian tropical cyclone data, but also to demonstrate the ability of the designed AI solution to produce insights on any one of the  $4.737 \times 10^{8234}$  possible scenarios  $((2.073 \times 10^{326}) \times (4.548 \times 10^{630}) \times (1.298 \times 10^{33}) \times (3.603 \times 10^{16}) \times (1.099 \times 10^{12}) \times (9.773 \times 10^{7215}) = 4.737 \times 10^{8234})$ .

In comparison with the existing literature in [8,9,15–18], this paper reports a unique system where the strategic decision-maker can use their own devices to select a particular scenario and immediately execute the best suited algorithms automatically, with outcomes reported in plain language. Using the latest technological innovations in AI-based Natural Language Processing (NLP) [32], AI-driven insights (i.e., the outcomes of AI algorithms) are explained in a language that is easily understandable by decision-makers. In the previous section, we saw Item 25 of Table 1, explaining results in natural language using NLP: “When LONGITUDE is between 107.6 and 123.1, the average of Central Pressure decreases by 7.77”. Thus, decision-makers no longer need to rely on data scientists for explanations of linear or logistic regressions.

As shown in Figure 12, when the strategic decision-maker selects a scenario, the proposed solution immediately filters the data and draws relationships with correlation coefficients on the filtered data. These figures demonstrate AI-based insights on relationships between critical cyclone-related parameters such as maximum speed, center pressure, wind gust, etc. The system hides the complex AI-based calculations from the user. Thus, this system is perfectly suitable for a strategic decision-maker who does not have any background in data analysis, AI, or mathematical modelling.

Unlike the statistical method of regression analysis (as shown in [33] to ascertain tornado damage ratings), AI-based regression analysis (demonstrated in this paper) is an end-to-end automated process (i.e., without the intervention of a data scientist), where plotting the relationship curves and describing the relationship in natural language (using NLP) is a completely automated process.

Although none of the existing research on tornadoes [8,9,15–18,33] demonstrated applicability of their solutions through mobile apps on mobile devices or tablets, the current solution can be deployed in a range of devices, including mobile devices, tablets, and traditional desktop computers. Figure 12 shows the app deployed on an Android app on a Samsung Galaxy 10 Lite mobile phone. It can also be deployed using iOS or Windows devices, with techniques shown in [6–12,22,23,34,35].

The regression, clustering, and CNN algorithm that were described in this paper for the analysis of Australian cyclones can also be used in analyzing various other disasters, as demonstrated in recent studies [6–12,22,23,34,35]. For example, we analyzed landslides in [6,7,10], tornadoes in [8,9], global events in [22–24], and even COVID-19 in [34,36]. In our previous studies [11,12], natural disasters such as earthquakes, bushfires, floods, volcanoes, droughts, tsunamis, etc. were successfully analyzed with higher levels of accuracy. These AI-based algorithms could be seamlessly integrated into any dataset, whether global [6,7] or local [8–10]. However, researchers need to understand which algorithms need to be used to solve which problem and use these algorithms in an appropriate manner suiting various preconditions, as shown in Table 4.

**Table 4.** Preconditions and purpose of using regression, clustering, and CNN-based anomaly detection in other research.

Name of Algorithm	Applicability	Pre-Condition
Linear regression	Finding out the factors that drive the metric being analyzed. Analyzes the dataset, ranks the factors that matter, and displays them as key influencers.	Supports only numeric values
Logistic regression	Finding out the factors that drive the metric being analyzed. Analyzes the dataset, ranks the factors that matter, and displays them as key influencers.	Supports only categorical values
Clustering	Finding out similarities or dissimilarities among categorical values by grouping	Supports only 1 dimension/categorical value and up to 15 measures/numeric values
CNN-based anomaly detection	Automatically detects anomalies in time series data. Provides explanations for anomalies to help with root cause analysis.	Supports only time series data

## 5. Conclusions

This paper presented an innovative solution for obtaining AI-driven answers to critical strategic questions on Australian tropical cyclones. By deploying automated regression (i.e., both linear and logistic regressions), k-means clustering, and CNN-based anomaly detection, the presented approach generates NLP-based insights in plain English for decision-makers. A strategic decision-maker can obtain AI-driven insights on their own mobile devices (i.e., iOS, Android, or Windows) for making evidence-based decisions.

This study not only presented an innovative and sustainable solution for comprehending Australian tropical cyclones, but also demonstrated the robustness of such a system by supporting an exhaustive scenario set of  $4.737 \times 10^{8234}$ . Moreover, we reported the experimentation and fine-tuning of the present system under varying levels of sensitivity (as shown in Table 3).

This study predominantly analyzed only two cyclone-related parameters such as central pressure and maximum air speed (out of 80 cyclone-related parameters available in the source data [13,14]). Although regression and clustering algorithms were used to analyze central pressure dynamics, CNN-based anomaly detection was used to analyze central pressure of Australian cyclones. There are many more critical parameters such as longitude, latitude, imagery, etc. corresponding to geospatial analysis that were outside the scope of this study (as demonstrated in [19,37]). Moreover, important cyclone-related analyses such as cyclone prediction, rainfall prediction, landfall prediction, detecting cyclones of unprecedented scale, and cyclone damage analysis were not investigated in this study (as demonstrated in [17,18,38–40]).

For future studies, focusing on a larger set of data with a wider range of attributes containing fewer empty values would be beneficial. Moreover, we endeavor to combine this tornado event-based dataset with social media-based tornado data (as reported in our

recent study [11]) for performing deep learning on more cyclone-related parameters with geospatial analysis.

**Author Contributions:** Conceptualization, F.S. and E.A.; methodology, F.S.; software, F.S.; validation, F.S. and M.A.; formal analysis, F.S. and E.A.; investigation, F.S., E.A. and M.A.; resources, F.S. and M.A.; data curation, F.S. and E.A.; writing—original draft preparation, F.S.; writing—review and editing, F.S. and E.A.; visualization, F.S.; funding acquisition, F.S. and M.A. All authors have read and agreed to the published version of the manuscript.

**Funding:** The authors would like to thank the Deanship of Scientific Research at Umm Al-Qura University for supporting this work by Grant Code: (22UQU4290525DSR03).

**Institutional Review Board Statement:** Not Applicable.

**Informed Consent Statement:** Not Applicable.

**Data Availability Statement:** Publicly available datasets were analyzed in this study [13]. Microsoft Power BI tool [21] was used to analyze the data with ESRI ArcGIS map, Line Chart, Bar Chart, Pie Chart and Key Influencers visualizations.

**Acknowledgments:** The authors would like to thank the Deanship of Scientific Research at Umm Al-Qura University for supporting this work by Grant Code: (22UQU4290525DSR03). Moreover, the authors would like to thank Taufiqur Rahman, a development expert working for Federal Government, Canberra, ACT, Australia for his support during the development of dashboards for this study.

**Conflicts of Interest:** The authors declare no conflict of interest.

## References

1. Australian Business Roundtable. Natural Disaster Costs to Reach \$39 Billion Per Year by 2050. 2021. Available online: <http://australianbusinessroundtable.com.au/assets/reports/media-release-nov-11.pdf> (accessed on 6 June 2022).
2. Australian Business Roundtable. Special Report: Update to the Economic Costs of Natural Disasters in Australia. 2021. Available online: <http://australianbusinessroundtable.com.au/our-research> (accessed on 6 June 2022).
3. United Nations. Early Warning Systems. Available online: <https://www.un-spider.org/risks-and-disasters/early-warning-systems#no-back> (accessed on 30 November 2021).
4. Alam, E.; Bhuiyan, R. Tornado hazard in Bangladesh: Nature, loss and coping. *Chittagong Univeristy J. Sci.* **2005**, *29*, 97–104.
5. World Bank. Economics for Disaster Prevention and Preparedness in Europe. 4 June 2021. Available online: <https://www.worldbank.org/en/news/feature/2021/06/04/economics-for-disaster-prevention-and-preparedness-in-europe> (accessed on 2 December 2021).
6. Sufi, F.K.; Alsulami, M. Knowledge Discovery of Global Landslides Using Automated Machine Learning Algorithms. *IEEE Access* **2021**, *9*, 131400–131419. [CrossRef]
7. Sufi, F.K. AI-Landslide: Software for acquiring hidden insights from global landslide data using Artificial Intelligence. *Softw. Impacts* **2021**, *10*, 100177. [CrossRef]
8. Sufi, F.; Alam, E.; Alsulami, M. A New Decision Support System for Analyzing Factors of Tornado Related Deaths in Bangladesh. *Sustainability* **2022**, *14*, 6303. [CrossRef]
9. Sufi, F.K. AI-Tornado: An AI-based Software for analyzing Tornadoes from disaster event dataset. *Softw. Impacts* **2022**, *11*, 100357. [CrossRef]
10. Sufi, F.; Alam, E.; Islam, A. A Scenario-based Case Study: AI to analyse casualties from landslides in Chittagong Metropolitan Area, Bangladesh. *Nat. Hazards Earth Syst. Sci. Dis.* **2022**, preprint.
11. Sufi, F.; Khalil, I. Automated Disaster Monitoring from Social Media Posts using AI based Location Intelligence and Sentiment Analysis. *IEEE Transactions on Computational Social Systems*, 2022; in press. [CrossRef]
12. Sufi, F.K. AI-SocialDisaster: An AI-based software for identifying and analyzing natural disasters from social media. *Softw. Impacts* **2022**, *11*, 100319. [CrossRef]
13. Australian Government, Bureau of Meteorology. Tropical Cyclone Databases. 2022. Available online: <http://www.bom.gov.au/cyclone/tropical-cyclone-knowledge-centre/databases/> (accessed on 6 June 2022).
14. Australian Government, Bureau of Meteorology. Tropical Cyclone Database: Structure Specification. 2022. Available online: [http://www.bom.gov.au/cyclone/history/database/TC\\_Database\\_Structure\\_Oct2011.pdf](http://www.bom.gov.au/cyclone/history/database/TC_Database_Structure_Oct2011.pdf) (accessed on 6 June 2022).
15. Nicholls, N.; Landsea, C.; Gill, J. Recent trends in Australian region tropical cyclone activity. *Meteorol. Atmos. Phys.* **1998**, *65*, 197–205. [CrossRef]
16. Dare, R.A.; Davidson, N.E. Characteristics of Tropical Cyclones in the Australian Region. *Mon. Weather Rev.* **2004**, *132*, 3049–3065. [CrossRef]

17. Aleskerov, F.; Demin, S.; Richman, M.B.; Shvydun, S.; Trafalis, T.B.; Yakuba, V. Constructing an Efficient Machine Learning Model for Tornado Prediction. *Int. J. Inf. Technol. Decis. Mak.* **2020**, *19*, 5. [CrossRef]
18. Diaz, J.; Joseph, M.B. Predicting property damage from tornadoes with zero-inflated neural networks. *Weather Clim. Extrem.* **2019**, *25*, 100216. [CrossRef]
19. Chen, Z.; Wagner, M.; Das, J.; Doe, R.K.; Cervený, R.S. Data-Driven Approaches for Tornado Damage Estimation with Unpiloted Aerial Systems. *Remote Sens.* **2021**, *13*, 1669. [CrossRef]
20. Ferrari, A. The Importance of Star Schemas in Power BI. Available online: <https://www.sqlbi.com/articles/the-importance-of-star-schemas-in-power-bi/> (accessed on 2 June 2021).
21. Microsoft Power, B.I. Download Power BI Desktop. 2021. Available online: <https://app.powerbi.com/> (accessed on 1 August 2022).
22. Sufi, F.K.; Alsulami, M. Automated Multidimensional Analysis of Global Events With Entity Detection, Sentiment Analysis and Anomaly Detection. *IEEE Access* **2021**, *9*, 152449–152460. [CrossRef]
23. Sufi, F.K. AI-GlobalEvents: A Software for analyzing, identifying and explaining global events with Artificial Intelligence. *Softw. Impacts* **2021**, *11*, 100218. [CrossRef]
24. Sufi, F.K. Identifying the drivers of negative news with sentiment, entity and regression analysis. *Int. J. Inf. Manag. Data Insights* **2022**, *2*, 100074. [CrossRef]
25. Dube, K.; Chapungu, L.; Fitchett, J. Meteorological and Climatic Aspects of Cyclone Idai and Kenneth. In *Cyclones in Southern Africa*; Sustainable Development Goals Series; Springer: Cham, Switzerland, 2021.
26. Yu, H.-F.; Hsieh, C.-J.; Chang, K.-W.; Lin, C.-J. Large Linear Classification When Data Cannot Fit in Memory. In Proceedings of the KDD'10: 16th ACM SIGKDD International Conference on Knowledge Discovery and Data Mining, Washington, DC, USA, 24–28 July 2010.
27. Matthies, H.; Strang, G. The solution of non linear finite element equations. *Int. J. Numer. Methods Eng.* **1979**, *14*, 1613–1626. [CrossRef]
28. Nocedal, J. Updating Quasi-Newton Matrices with Limited Storage. *Math. Comput.* **1980**, *35*, 773–782. [CrossRef]
29. Ren, H.; Xu, B.; Wang, Y.; Yi, C.; Huang, C.; Kou, X.; Xing, T.; Yang, M.; Tong, J.; Zhang, Q. Time-Series Anomaly Detection Service at Microsoft. In Proceedings of the KDD'19: 25th ACM SIGKDD International Conference on Knowledge Discovery & Data Mining, Anchorage, AK, USA, 4–8 August 2019.
30. Zhao, R.; Ouyang, W.; Li, H.; Wang, X. Saliency detection by multi-context deep learning. In Proceedings of the IEEE Conference on Computer Vision and Pattern Recognition, Boston, MA, USA, 7–12 June 2015.
31. Microsoft Documentation. Choosing a Natural Language Processing Technology in Azure. 25 February 2020. Available online: <https://docs.microsoft.com/en-us/azure/architecture/data-guide/technology-choices/natural-language-processing> (accessed on 21 August 2021).
32. Microsoft Documentation. What Is Language Detection in Azure Cognitive Service for Language? 30 July 2022. Available online: <https://docs.microsoft.com/en-us/azure/cognitive-services/text-analytics/language-support?tabs=language-detection> (accessed on 1 August 2022).
33. Elsner, J.B.; Schroder, Z. Tornado Damage Ratings Estimated with Cumulative Logistic Regression. *J. Appl. Meteorol. Climatol.* **2019**, *58*, 2733–2741. [CrossRef]
34. Sufi, F.; Alsulami, M. AI-based Automated Extraction of Location-Oriented COVID-19 Sentiments. *Comput. Mater. Contin. CMC* **2022**, *72*, 3631–3649.
35. Sufi, F.; Alsulami, M. A Novel Method of Generating Geospatial Intelligence from Social Media Posts of Political Leaders. *Information* **2022**, *13*, 120. [CrossRef]
36. Sufi, F.; Razzak, I.; Khalil, I. Tracking Anti-Vax Social Movement Using AI based Social Media Monitoring. *IEEE Transactions on Technology and Society*, 2022; in press. [CrossRef]
37. Paliwal, M.; Patwardhan, A. Analysis of Cyclone Tracks of North Indian Ocean Using Cluster Analysis. In *Monitoring and Prediction of Tropical Cyclones in the Indian Ocean and Climate Change*; Springer: Dordrecht, The Netherlands, 2014; pp. 89–96.
38. Richman, M.B.; Leslie, L.M.; Ramsay, H.A.; Klotzbach, P.J. Reducing Tropical Cyclone Prediction Errors Using Machine Learning Approaches. *Procedia Comput. Sci.* **2017**, *114*, 314–323. [CrossRef]
39. European Commission Joint Research Centre. Tropical Cyclone IDAI: Analysis of the Wind, Rainfall and Storm Surge Impact. 9 April 2019. Available online: [https://www.humanitarianresponse.info/sites/www.humanitarianresponse.info/files/documents/files/joint\\_research\\_centre\\_analysis\\_of\\_wind\\_rainfall\\_and\\_storm\\_surge\\_impact\\_09\\_april\\_2019.pdf](https://www.humanitarianresponse.info/sites/www.humanitarianresponse.info/files/documents/files/joint_research_centre_analysis_of_wind_rainfall_and_storm_surge_impact_09_april_2019.pdf) (accessed on 1 August 2022).
40. Wang, Z.; Zhao, J.; Huang, H.; Wang, X. A Review on the Application of Machine Learning Methods in Tropical Cyclone Forecasting. *Front. Earth Sci.* **2022**, *10*, 902596. [CrossRef]